Examining the role of different molecular interactions on activation energies and activation volumes in liquid water

Zeke A. Piskulich* and Ward H. Thompson*

Department of Chemistry, University of Kansas, Lawrence, KS 66045, USA

E-mail: piskuliche@ku.edu; wthompson@ku.edu

June 1, 2021

Abstract

There are a large number of force fields available to model water in molecular dynamics simulations, which each have their own strengths and weaknesses in describing the behavior of the liquid. One particular weakness in many of these models is their description of dynamics away from ambient conditions, where their ability to reproduce measurements is mixed. To investigate this issue we use the recently developed fluctuation theory for dynamics to directly evaluate measures of the local temperature and pressure dependence: the activation energy and the activation volume. We examine these activation parameters for hydrogen-bond jump exchange times, OH reorientation times, and diffusion coefficients calculated from the SPC/E, SPC/Fw, TIP3P-PME, TIP3P-PME/Fw, OPC3, TIP4P/2005, TIP4P/Ew, E3B2, and E3B3 water models. Activation energy decompositions available through the fluctuation theory approach provide mechanistic insight into the origins of different temperature dependences between the various models, as well as the influence of three-body effects and flexibility.

1 Introduction

Liquid water plays a vital role in many processes in chemistry and biology. It is thus of no surprise that a plethora of approaches have been developed to describe its interactions in the neat liquid,[1–4] in solution,[5] and near proteins.[6–8] These models are typically developed to recreate a specific subset of the features of liquid water (*e.g.*, density maximum, melting temperature, vaporization enthalpy), sometimes at the expense of other properties. Regardless of these limitations, empirical water models have been widely successful in developing our understanding of water as a neat liquid,[9–16] under extreme conditions,[17–20] and in complex environments.[21–26]

Most water models, however, do not directly incorporate dynamical quantities into their parameter optimization and even fewer use the temperature or pressure dependence of these quantities.[2,27–29] These dependencies are omitted both because their inclusion would significantly increase the complexity of fitting force-field parameters and the difficulty of computing the properties, *e.g.*, the modification of dynamical timescales with pressure typically requires precise calculations over a large range of pressures. This has led to a situation where many empirical water models accurately describe the self-diffusion coefficient in the bulk liquid at 298.15 K and 1 bar but display variable success in reproducing the behavior under other conditions. Activation energies and volumes are the

key measures of the temperature and pressure dependence of dynamical timescales, indicating how they behave at nearby conditions.

The activation energy of a dynamical timescale τ,

$$E_a = -\frac{\partial \ln(1/\tau)}{\partial \beta}, \tag{1}$$

where $\beta = 1/(k_b T)$ with k_b Boltzmann's constant and T temperature, represents the first-order description of the timescale's temperature dependence. Typically, activation energies are calculated numerically from experimental or simulation T-dependent data using the Arrhenius equation, $k(T) = A\, e^{-\beta E_a}$, where the prefactor A and E_a are assumed to be temperature independent.

Similarly, the activation volume of a timescale,

$$\Delta V^{\ddagger} = -k_b T \frac{\partial \ln(1/\tau)}{\partial p}, \tag{2}$$

is the first-order description of the timescale's dependence on the pressure p. As is the case for the activation energies, a numerical approach involving experiments or simulations over a range of pressures is typically used.[30–32] However, such an analysis can be significantly more complicated because large pressure ranges – on the order of thousands of bar – are often required to resolve changes in the timescale.

While both activation parameters provide only a local viewpoint of the T and p dependence of these timescales and ignore non-Arrhenius effects, they are the primary contributors to these dependence and thus must be accurate for a model to perform well at other conditions.

In this Paper, we examine three key timescales for liquid water – the H-bond exchange, or "jump" time, the OH reorientation time, and the self-diffusion coefficient – and the corresponding activation parameters for the SPC/E,[1] SPC/Fw,[2] TIP3P-PME,[6,33] TIP3P-PME/Fw,[6,33] OPC3,[27] TIP4P/Ew,[4] TIP4P/2005,[3] E3B2,[28] and E3B3[29] water models using the recently developed fluctuation theory for dynamics.[34–42] This method allows E_a and $\Delta V^{\ddagger}$ to be calculated directly using simulations at a single temperature and pressure rather than the numerical Arrhenius approach. Thus, it provides the activation energy and activation volume to high precision. In addition, it provides a route to otherwise unavailable mechanistic information through a rigorous decomposition of the activation energy into components associated with the motions and interactions present in the system.

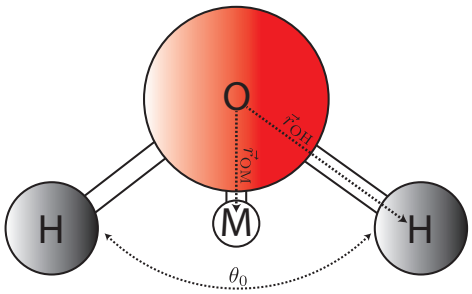

Figure 1: Schematic diagram of interaction sites for the water force fields.

2 Computational Methods

2.1 Force Fields

In the present work we have selected several commonly used water force fields[1–4,6,27–29,33] used in molecular dynamics (MD) simulations. These include three- and four-site models, rigid and flexible models, and some that include three-body effects. While these models reflect only a small subset of the vast number of available force fields, they are widely used in describing water in the neat liquid, in complex environments, and in biomolecular simulations.

All of the models use an oxygen-oxygen Lennard-Jones potential to describe the van der Waals interactions,

$$U_{LJ}(r_{OO}) = 4\epsilon_{OO}\left[\left(\frac{\sigma_{OO}}{r_{OO}}\right)^{12} - \left(\frac{\sigma_{OO}}{r_{OO}}\right)^{6}\right], \tag{3}$$

where r_{OO} is the O–O distance, ϵ_{OO} the depth of the well, and σ_{OO} the site diameter. Note, each of the present calculations also use the long-range tail corrections to the energy and pres-

Table 1: Force field parameters used for each of the water models.

Water Model	σ_{OO} (Å)	ϵ_{OO} (kcal/mol)	q_O (e)	q_H (e)	r_0 (Å)	k_{OH} (K)	θ_0 (degrees)	k_θ (K)	r_{OM} (Å)	q_M (e)
SPC/E[1]	3.166	0.155	-0.8476	0.4238	1.0	-	109.47	-	-	-
SPC/Fw[2]	3.165	0.155	-0.82	0.41	1.012	1059.162	113.24	75.90	-	-
TIP3P-PME[6,33]	3.188	0.102	-0.83	0.415	0.9572	-	104.52	-	-	-
TIP3P-PME/Fw[6,33]	3.188	0.102	-0.83	0.415	0.9572	900	104.52	110	-	-
OPC3[27]	3.17427	0.16341	-0.89517	0.447585	0.97888	-	109.47	-	-	-
E3B2[28]	3.1536	0.1550	0.0	0.520	0.9572	-	104.52	-	0.1550	-1.040
E3B3[29]	3.1589	0.1852	0.0	0.5564	0.9572	-	104.52	-	0.1546	-1.1128
TIP4P/2005[3]	3.1589	0.1852	0.0	0.5564	0.9572	-	104.52	-	0.1546	-1.1128
TIP4P/Ew[4]	3.16435	0.16275	0.0	0.5242	0.9572	-	104.52	-	0.1250	-1.0484

Note: σ_{HH} and ϵ_{HH} are zero for all models.

Water Model	$\mathcal{E}_2$ kcal/mol	k_2 Å^{-1}	$\mathcal{E}_a$ kJ/mol	$\mathcal{E}_b$ kJ/mol	$\mathcal{E}_c$ kJ/mol	k_3 Å^{-1}
E3B2	2.349×10^6	4.872	1745.7	-4565.0	7606.8	1.907
E3B3	0.453×10^6	4.872	150.0	-1005.0	1880.0	1.907

sure described by Sun.[43] The electrostatic interactions are calculated using Coulomb's law, as

$$U_{Elec}(r_{ij}) = \sum_i \sum_j \frac{q_i\, q_j}{4\pi\epsilon_0 r_{ij}}, \qquad (4)$$

where q_i and q_j are the charges of the i^{th} and j^{th} atoms separated by distance r_{ij}, and ϵ_0 is the permitivity of free space. The long-range electrostatics are described using the Particle-Particle-Particle-Mesh Ewald (PPPM) summation method.[44,45] We have included in Table 1 the potential parameters for each model investigated in the present work.

In three of the water models studied (SPC/E, TIP3P-PME, and OPC3) the molecular interactions are fully described by Eqs. (3) and (4) with the SHAKE algorithm[46] used to hold the bonds and angles at their equilibrium values.

Two other models (SPC/Fw and TIP3P-PME/Fw) incorporate flexibility in the form of harmonic bond stretches and angle bends, as

$$U_{bond}(r_{OH}) = \frac{1}{2} k_{OH}\,(r_{OH} - r_0)^2, \qquad (5)$$

and

$$U_{angle}(\theta) = \frac{1}{2} k_\theta\,(\theta_{HOH} - \theta_0)^2, \qquad (6)$$

where k_{OH} (k_θ) is the bond (angle) force constant, r_{OH} (θ_{HOH}) is the instantaneous bond length (angle), and r_0 (θ_0) is the equilibrium bond length (angle). For SPC/Fw the force field was obtained by a reparameterization of the SPC/E Lennard-Jones parameters while adding flexibility,[2] while for TIP3P-PME/Fw flexibility was added without other changes from the TIP3P-PME parameters.[6,33] It should be noted that the PME variant of TIP3P uses the corrected parameters developed by Price and Brooks in Ref. 33 which account for the inclusion of long-range electrostatics in the calculations. Previous studies indicate that the original TIP3P parameterization has even faster dynamics than TIP3P-PME.[6,33]

Two additional models use a 4-site description of water (TIP4P/Ew and TIP4P/2005) in which the oxygen retains its Lennard-Jones site but the oxygen charge is moved a distance r_{OM} away from the oxygen atom along the bisector of the HOH angle between the hydrogen atoms. This is depicted schematically in Fig. 1. These interactions are still calculated from Eqs. (3) and (4), but with the modified oxygen charge position.

The models listed above are completely pairwise, with many-body effects included only in an average way by virtue of the fitting to experimental data. The E3B models developed by Tainter *et al.*[28,29] are built on top of existing 4-site descriptions of the pairwise interactions to include explicit three-body cooperativity as part of the model. The total potential energy of each E3B model may be written in terms of

the above equations as

$$U_{E3B} = U_{base} + U_2 + U_{3-body}, \tag{7}$$

where here U_{base} is the potential energy described by the TIP4P model (E3B2) or the TIP4P/2005 model (E3B3).

This first term in the three-body part,

$$U_2(r_{ij}) = \mathcal{E}_2 \sum_{i,j} e^{-k_2 r_{ij}}, \tag{8}$$

removes the many-body interactions typically built into two-body potentials implicitly. Here $\mathcal{E}_2$ and k_2 are constants and r_{ij} is the distance between the two oxygen atoms. The explicit 3-body part of the potential is

$$U_{3-body} = U_A + U_B + U_C \tag{9}$$

where A, B, and C are labels for anti-cooperative double H-bond donor interactions (central water donates H-bonds to two other waters), cooperative interaction of molecules that donate and accept an H-bond (central water donates to one water, accepts from another), and the anti-cooperative double H-bond acceptor interactions (central water accepts from two other waters), respectively. These three configurations are illustrated below in Fig. 4. The terms U_A, U_B, and U_C are calculated as

$$U_X = \mathcal{E}_X \sum_{i,j,k,l} f(r_{ij}) f(r_{kl}), \tag{10}$$

where $X = A$, B, or C, and r_{ij} and r_{kl} are the $H_d \cdots O_a$ hydrogen bond distances connecting the central water molecule to the two other water molecules in the triad interaction.

The function $f(r)$ is given by

$$f(r) = e^{-k_3 r}\, s(r), \tag{11}$$

where $s(r)$ is the switching function,

$$s(r) = \begin{cases} 1 & r < r_s \\ \frac{(r_f - r)^2 (r_f + 2r - 3r_s)}{(r_f - r_s)^3} & r_s \le r \le r_f \\ 0 & r > r_f \end{cases} \tag{12}$$

which smoothly truncates the calculation of 3-body interactions at OH distances between $r_s =$ 5.0 Å and $r_f =$ 5.2 Å. This term is included because the summations in Eqs. (9) and (10) include 42 terms, which fall off nearly to zero beyond 5.0 Å, thus these terms are excluded at greater distances for computational efficiency.

2.2 Fluctuation Theory

Recently, we have shown how the temperature and pressure dependence for a general property can be obtained from simulations at a single p and T using fluctuation theory for dynamics.[34–42] To illustrate the approach, we can consider a general time-dependent property, $f(t)$, and its average in the isobaric-isothermal (NpT) ensemble, $\langle f(t) \rangle$. It is straightforward to show that the temperature derivative of the average is given by

$$\frac{\partial \langle f(t) \rangle}{\partial \beta} = -\langle [\delta H(0) + p\, \delta V(0)]\, f(t) \rangle, \tag{13}$$

where $\delta H(0) = H(0) - \langle H \rangle$ and $\delta V(0) = V(0) - \langle V \rangle$ are the fluctuations in energy and volume, respectively, at $t = 0$. We note that at 1 bar, the $p\,\delta V$ term is approximately $10^4 - 10^5$ times smaller than the $\delta H(0)$ contribution and thus can be neglected at low pressures. Thus, in this work we take

$$\frac{\partial \langle f(t) \rangle}{\partial \beta} = -\langle \delta H(0) f(t) \rangle. \tag{14}$$

The pressure derivative can similarly be expressed as[47]

$$\frac{\partial \langle f(t) \rangle}{\partial p} = -\beta \langle \delta V(0) f(t) \rangle. \tag{15}$$

A key feature of the expressions in Eqs. (14) and (15) is that they can be evaluated from the same simulations, at a single p and T, used to calculate $\langle f(t) \rangle$ itself. That is, they are the analytical derivatives with respect to β and p in contrast to the numerical derivative obtained from an Arrhenius analysis in either T or p.

In the following, we describe how this dynamical fluctuation theory can be straightforwardly applied to determine the temperature and pressure dependence of the diffusion coef-

ficient, the OH reorientation time, and the H-bond exchange jump time.

2.2.1 Diffusion Coefficients

A key measure of water dynamics is contained in the self-diffusion coefficient, D, which can be obtained experimentally from quasi-elastic neutron scattering,[48] tracer studies,[49,50] or Nuclear Magnetic Resonance (NMR) measurements.[51–54] In MD simulations, the diffusion coefficient is obtained from the long-time behavior of the average mean-squared displacement, $\langle MSD(t)\rangle = \langle|\vec{r}(0) - \vec{r}(t)|^2\rangle$,

$$D = \lim_{t\to\infty} \frac{\langle MSD(t)\rangle}{6t}, \tag{16}$$

where $\vec{r}(t)$ is the molecule position, here defined by the location of the oxygen atom, at time t.

Taking the derivative of D in Eq. (16) with respect to β gives a result analogous to that in Eq. (14),

$$\frac{\partial D}{\partial \beta} = -\lim_{t\to\infty} \frac{\langle \delta H(0)\,|\vec{r}(0) - \vec{r}(t)|^2\rangle}{6t}, \tag{17}$$

so that the activation energy associated with the diffusion coefficient is

$$E_{a,D} = \frac{\lim_{t\to\infty}\langle \delta H(0)\,|\vec{r}(0) - \vec{r}(t)|^2\rangle}{\lim_{t\to\infty}\langle|\vec{r}(0) - \vec{r}(t)|^2\rangle}. \tag{18}$$

In practice, the ratio of the slopes (at long times) of the numerator and denominator are used to determine $E_{a,D}$. Analogous results are obtained for the pressure derivative giving

$$\Delta V_D^{\ddagger} = \frac{\lim_{t\to\infty}\langle \delta V(0)\,|\vec{r}(0) - \vec{r}(t)|^2\rangle}{\lim_{t\to\infty}\langle|\vec{r}(0) - \vec{r}(t)|^2\rangle}. \tag{19}$$

for the activation volume for diffusion.

It is well known that D is underestimated in periodic-boundary condition (PBC) simulations such as those used here. This can be corrected using[55,56]

$$D = D_{PBC} + \frac{2.837297 k_B T}{6\pi\eta_s L}, \tag{20}$$

where D_{PBC} is the value calculated from Eq. (16) in PBC simulations, η_s is the shear viscosity, and L is the side length of the PBC simulation cell. From a simulation, the shear viscosity is evaluated from the Green-Kubo relation,

$$\eta_s = \frac{V}{k_B T}\int_0^\infty \langle P_{\alpha\beta}(0) P_{\alpha\beta}(t)\rangle \mathrm{dt}, \tag{21}$$

where here the repeated $\alpha\beta$ subscript denotes an average of the five correlation functions constructed from the stress tensor: $(P_{xx} - P_{yy})/2$,$(P_{yy} - P_{zz})/2$, P_{xy}, P_{yz}, and P_{xz}. We have previously shown $E_{a,D}$ is unaffected by this correction if the Stokes-Einstein relation holds and only minimally affected if it does not,[38] so no corrections are used.

We have previously reported diffusion activation energies for SPC/E and TIP4P/2005 water using this method[35,40] as well as activation volumes for TIP4P/2005 water.[47]

2.2.2 Reorientation Times

The OH reorientational dynamics of water are most frequently characterized by the second-order reorientation time correlation function (TCF),

$$C_2(t) = \langle P_2\left[\vec{e}_{OH}(0)\cdot\vec{e}_{OH}(t)\right]\rangle, \tag{22}$$

where $\vec{e}_{OH}$ is a unit vector along the OH bond and P_2 is the 2^{nd} Legendre polynomial. The dynamics can be measured by infrared pump-probe anisotropy experiments, which determine the anisotropy decay, $r(t) = 0.4C_2(t)$,[57] or NMR measurements that yield the average reorientation time given by the integral of $C_2(t)$.[58]

In water, $C_2(t)$ decays on three timescales which can be attributed to inertial, librational, and reorientation associated with H-bond dynamics. It is this last, denoted as τ_2, which is of greatest interest and the focus of the present work. The timescales can be obtained by fitting $C_2(t)$ to a tri-exponential function

$$C_2(t) = \sum_\alpha A_\alpha\, e^{-t/\tau_\alpha}, \tag{23}$$

where $\alpha = iner$, $libr$, and 2. Following Eqs. (14) and (15), it is straightforward to show that

$$\frac{\partial C_2(t)}{\partial \beta} = -\langle \delta H(0) P_2 \left[\vec{e}_{OH}(0) \cdot \vec{e}_{OH}(t) \right] \rangle, \quad (24)$$

and

$$\frac{\partial C_2(t)}{\partial p} = -\beta \langle \delta V(0) P_2 \left[\vec{e}_{OH}(0) \cdot \vec{e}_{OH}(t) \right] \rangle. \quad (25)$$

These derivative TCFs can be fit to the corresponding derivative of Eq. (23),

$$\frac{\partial C_2(t)}{\partial x} = \sum_\alpha \left[\frac{\partial A_\alpha}{\partial x} - A_\alpha t \frac{\partial (1/\tau_\alpha)}{\partial x} \right] e^{-t/\tau_\alpha}, \quad (26)$$

where $x = \beta$ or p. In the fitting, the amplitudes A_α and timescales τ_α are constrained to the values obtained in fitting $C_2(t)$ to Eq. (23) so that their derivatives are the fitting parameters. Given the timescale and its derivatives, the reorientational activation energy, $E_{a,2}$, and activation volume, $\Delta V_2^\ddagger$, can be obtained. We have previously calculated reorientation activation energies in this way for the SPC/E[35,41] and TIP4P/2005[36] models, but have never reported reorientation activation volumes.

2.2.3 H-bond Jump Times

The fundamental molecular mechanism underlying both diffusion and reorientation in water is the exchange of H-bond partners.[9,10,59] These exchanges, or "jumps," can be thought of as a kind of chemical reaction in which an OH group breaks one H-bond and forms another. The corresponding rate constant can be obtained from the stable-states, side-side, time correlation function,

$$C_{ab}(t) = \langle n_a(0)\, n_b(t) \rangle \quad (27)$$

where $n_a = 1$ ($n_b = 1$) if the OH is H-bonded to acceptor a (b). Thus, for an OH initially H-bonded to an acceptor labeled a, $C_{ab}(t)$ is zero at $t = 0$ when $n_a = 1$ and $n_b = 0$, but rises as OH groups switch to new acceptors. The time dependence is such that $1 - C_{ab}(t)$ decays with the jump time τ_0, which is the inverse of the rate constant for the H-bond exchange. In practice, there is also some small-amplitude, short-time dynamics not associated with the H-bond jumps so that $1 - C_{ab}(t)$ is accurately fit by Eq. (23) with two exponentials and the longer timescale equal to τ_0.

The derivatives of the stable-states TCF are obtained from Eqs. (14) and (15) as

$$\frac{\partial [1 - C_{ab}(t)]}{\partial \beta} = \langle \delta H(0)\, n_a(0)\, n_b(t) \rangle, \quad (28)$$

and

$$\frac{\partial [1 - C_{ab}(t)]}{\partial p} = \beta \langle \delta V(0)\, n_a(0)\, n_b(t) \rangle. \quad (29)$$

In analogy to the reorientational dynamics, these derivative TCFs can be fit to Eq. (26) to obtain $\partial(1/\tau_0)/\partial\beta$ and $\partial(1/\tau_0)/\partial p$ and then the jump time activation energy, $E_{a,0}$, and activation volume, $\Delta V_0^\ddagger$. It should be noted that for both reorientational and jump dynamics, finite simulation size effects are not expected to play as large a role as they do for diffusion due to the small volume of each water molecule.[60] We have recently carried out a detailed investigation of the jump activation energies for SPC/E water.[41]

2.2.4 Activation Energy Decompositions

A key feature of fluctuation theory for dynamics is the ability to decompose the activation energy by separating the energy fluctuation into components, *e.g.*, $\delta H = \delta KE + \delta U_{LJ} + \delta U_{Elec} + \delta U_{Bond} + \delta U_{Angle} + \delta U_2 + \delta U_{3-body}$. This allows the calculation of different contributions to the activation energy as

$$\begin{aligned} E_a &= E_a^{KE} + E_a^{LJ} + E_a^{Elec} \\ &+ E_a^{Bond} + E_a^{Angle} \\ &+ E_a^{U_2} + E_a^{3-body}. \end{aligned} \quad (30)$$

These different contributions to the activation energy can be understood in terms of Tolman's (rigorous) perspective in which the activation energy is equal to the average energy of reacting species minus the average energy of reactant

species.[61] That is, rather than the energy of the barrier itself, E_a is the energy required to overcome the barrier and hence is decomposable.

As an example, the kinetic energy contribution to the diffusion activation energy can be calculated by replacing $\delta H(0)$ with $\delta KE(0)$ in the derivative of the mean-squared displacement. Then, the kinetic energy contribution is given by

$$E_{a,D}^{KE} = \frac{\lim_{t\to\infty} \langle \delta KE(0) \, |\vec{r}(0) - \vec{r}(t)|^2 \rangle}{\lim_{t\to\infty} \langle |\vec{r}(0) - \vec{r}(t)|^2 \rangle}, \quad (31)$$

and can be interpreted as the average kinetic energy of diffusing molecules minus the average kinetic energy of all molecules.

Extracting activation energy contributions to the jump or reorientation derivative TCFs are likewise straightforward. The relevant component of the derivative of the timescale, *e.g.*, $\partial(1/\tau_0)/\partial\beta^{KE}$, is extracted as discussed by fitting the contribution TCF, *e.g.*, $\langle \delta KE(0)\, n_a(0)\, n_b(t) \rangle$ to Eq. (26) just as the total derivative TCF is fit. This derivative value is then used to calculate the activation energy component, $E_{a,0}^{KE} = (1/\tau_0)[\partial(1/\tau_0)/\partial\beta^{KE}]$.

2.3 Simulation Details

For each model, we used PACKMOL[62] to generate initial configurations and necessary data files for MD simulations. Initial velocities were generated from the room temperature Maxwell-Boltzmann distribution. Simulations were run using the Large-Scale Atomic/Molecular Massively Parallel Simulator (LAMMPS).[63] An isothermal-isobaric, NpT, ensemble trajectory was propagated at 1 bar and 298.15 K for 1 ns to reach equilibrium, and then production simulations were run for 50 ns.[64,65] A Nosé-Hoover thermostat and barostat were used, both of chain length 3, with damping parameters of 100 fs and 1000 fs, respectively.[66,67] From these production simulations, configurations and velocities were output every 1 ps, for a total of 50,000 configurations for each water model.

From each of these saved configurations a 20 ps constant energy, NVE, simulation was propagated with configurations dumped every 10 fs, from which the TCFs were calculated. Reported values were obtained by averaging these TCFs across all 50,000 trajectories, and then fitting these averaged results. Similarly, derivative correlation functions were calculated in the same way with each trajectory's contribution to the average weighted by the fluctuation in the energy. Uncertainties in the fluctuation calculation are reported using block averaging over 10 blocks, and represent a 95% confidence interval according to Student's t-distribution.[68]

We have additionally calculated the viscosity of each water model from additional MD simulations. For these simulations, five sets of equilibrium configurations and velocities were used as starting points for 1 ns NVT simulations, from which viscosities were calculated using the Green-Kubo formalism described in Sec. 2.2.1. Each trajectory was used as a block for block averaging and values are again reported as a 95 % confidence interval. For TIP3P-PME/Fw the pressure tensor was output every 4 ps as it was required to accurately capture the oscillations in the correlation function. For all other models the pressure tensor was output every 10 ps. For all models the viscosity time-correlation function was calculated over 5 ps, with time origins separated every 100 fs.

For all simulations, the timestep was 1 fs and the PPPM method[44,45] was used for the calculation of electrostatic interactions, with a tolerance parameter of 1×10^{-4}. For simulations involving rigid water molecules, the SHAKE algorithm[46] was used to hold bonds and angles constant, also with a tolerance of 1×10^{-4}.

3 Results and Discussion

We have evaluated the jump time τ_0, the reorientation time τ_2, and the diffusion coefficient D along with their activation energies and volumes calculated using dynamical fluctuation theory. In the following, we present and discuss the values obtained for these properties from the different water models and compare with available experimental results.

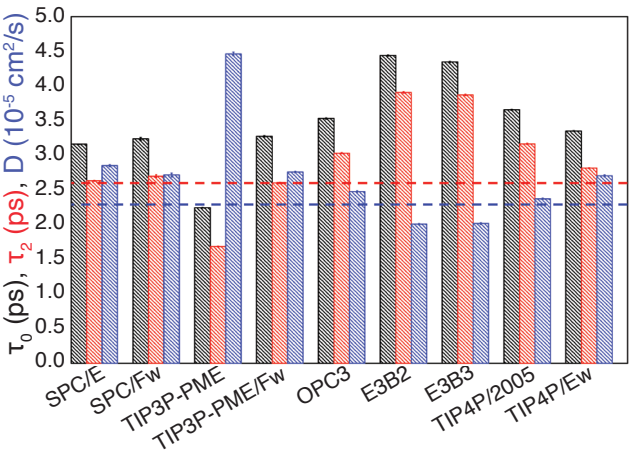

Figure 2: The H-bond jump time τ_0 (black), OH reorientation time τ_2 (red), and diffusion coefficient D (blue) are presented for each water model. Experimental values for the reorientation time[69–71] (red dashed line) and diffusion coefficient[72] (blue dashed line) are also included.

3.1 Timescales

We begin by examining the jump time, reorientation time, diffusion coefficient, and viscosity calculated from the simulations described in Sec. 2 for each studied force field. We have reported these timescales for each model in Table 2 and plotted them in Fig. 2. The values are in excellent agreement with previous reported simulations results in the literature.[2–4,27,33,74–77] For comparison, we have included available experimental literature results, Note that pump-probe IR anisotropy results have yielded $\tau_2 =$ 2.5,[69] 2.6,[70] and 2.7 ps;[71] in the following we use the average of these results, 2.6 ps, as the experimental value.

We first consider the rigid 3-site water models, SPC/E, TIP3P-PME, and OPC3. These models give some of the shortest reorientation and jump times and some of the largest diffusion coefficients. In particular, the τ_2 value predicted by the SPC/E (2.63 ps) model is in excellent agreement with the measured result of 2.6 ps. In contrast, the OPC3 (3.03 ps) predicts slower dynamics than measured while the TIP3P-PME reorientation time of 1.67 ps is dramatically lower.

The H-bond jump time cannot be directly extracted from experimental measurements and thus we do not have an unambiguous way to use it to test the models. However, because the OH reorientation time is dominated by the timescale for H-bond jumps,[9,10] it is a reasonable assumption that the models which describe τ_2 well should yield the most accurate jump time. This yields an inference that the "experimental" τ_0 is approximately $3.2 - 3.3$ ps, based on the SPC/E, SPC/Fw, and TIP3P-PME/Fw results.

The diffusion coefficients for the rigid 3-site models overestimate the experimental value. The SPC/E and OPC3 do so modestly, yielding values that are 24 and 8% larger than the measured D. As with the other timescales, the TIP3P-PME model predicts grossly accelerated diffusive dynamics with D more than 93% too big. The viscosities of these models are consistent with this as they have significantly lower values than that reported experimentally.[73] It is certainly interesting that a model like SPC/E correctly predicts τ_2, but overestimates D. Both quantities have H-bond exchanges as the underlying process, but diffusion involves a component related to the size of the translational "jump" upon exchange[59] and perhaps it is this structural quantity that is not properly described within the SPC/E model.

The impact of the faster dynamics in the TIP3P-PME model should be clearly recognized given that it is one of the most frequently used models for biomolecular simulations. The present results indicate that not only does the TIP3P-PME model diffuse and reorient more quickly than real water as has been frequently reported in the literature,[7,78,79] it likely also exchanges H-bond partners more quickly than real water. This could have important implications for studies of processes influenced by these motions, *e.g.*, water dynamics involved in enzymatic reactions and in hydration of proteins.

Two of the models studied, SPC/Fw and TIP3P-PME/Fw, involve the addition of bond and angle flexibility to a rigid 3-site model. Interestingly, the addition of flexibility appears to fix many of the sins of the TIP3P-PME model. TIP3P-PME/Fw gives a reorientation time in perfect agreement with the experimental result and has a diffusion coefficient that

Table 2: H-bond jump time τ_0, OH reorientation time τ_2, diffusion coefficients directly from the simulations, D_{PBC}, and corrected for finite-size effects, D, and shear viscosities, η_s for different water models; times are in ps, diffusion coefficients are in 10^{-5} cm^2/s, and shear viscosities are in cP. Subscripts indicate uncertainties in the trailing digit(s).

Model	τ_0	τ_2	D_{PBC}	D	η_s
SPC/E	3.160_3	2.633_4	2.437_4	2.85_2	0.71_3
SPC/Fw	3.237_{20}	2.699_{21}	2.358_{18}	2.72_3	0.82_5
TIP3P-PME	2.245_3	1.686_7	3.823_6	4.46_3	0.46_2
TIP3P-PME/Fw	3.273_{10}	2.603_{10}	2.391_5	2.76_1	0.80_2
OPC3	3.531_7	3.031_8	2.120_4	2.48_1	0.82_2
E3B2	4.440_7	3.907_{11}	1.721_3	2.00_1	1.03_3
E3B3	4.346_7	3.871_{11}	1.727_4	2.02_2	1.01_4
TIP4P/2005	3.657_7	3.165_8	2.030_4	2.37_1	0.85_2
TIP4P/Ew	3.351_4	2.815_6	2.314_3	2.70_2	0.75_3
Expt.[69–73]	–	2.6		2.30	0.8903

is significantly more reasonable. Furthermore, the viscosity of TIP3P-PME/Fw is nearly double that of TIP3P-PME, bringing it in line with the other 3-site models studied. Interestingly, the SPC/Fw model, which both adds flexibility and reparameterizes the intramolecular interactions, provides only minimal differences in the timescales when compared with the SPC/E model though it does slightly increase the models viscosity.

Compared with the 3-site models, the dynamics of the 4-site models, TIP4P/2005 and TIP4P/Ew, are generally slower. We find OH reorientation times of 2.82 ps for TIP4P/Ew and 3.17 ps for TIP4P/2005, which are longer than the measured τ_2. This suggests that these models also overestimate the H-bond jump time. On the other hand, the TIP4P/2005 diffusion coefficient, 2.37×10^{-5} cm^2/s, is the closest to the experimental value out of all the force fields studied and TIP4P/Ew gives a reasonable result (2.70×10^{-5} cm^2/s). Likewise, the TIP4P/2005 viscosity is the closest to the experimental value of all the water models. Like the 3-site models, the 4-site model with the most accurate reorientation time, TIP4P/Ew, gives a diffusion coefficient that is too large, while the excellent prediction of D by TIP4P/2005 is accompanied by a reorientation time that is 22% larger than obtained in experiments.

The addition of 3-body interactions in the E3B2 and E3B3 models leads to slower dynamics compared to the pairwise 4-site models. They exhibit reorientation times that are too long by more $\sim$ 1.2 ps (50%) and diffusion coefficients that are underestimated, unlike all the other force fields considered. The predicted D are, however, quite reasonable, providing the second best agreement behind the TIP4P/2005 model (upon which the E3B3 model is based). The slower D than experiment is consistent with our calculated values of the viscosity, which indicate that both E3B variants are more viscous than experiment.

Overall, the results show that the best models to use to obtain the correct OH reorientation time at 298.15 K and 1 bar are the rigid 3-site SPC/E and the flexible variants SPC/Fw and TIP3P-PME/Fw. For diffusion, the TIP4P/2005 force field provides the most faithful reproduction of the experimental D.

3.2 Activation Energies

We next turn to an investigation of the temperature dependence of each water model as measured by the activation energies of the jump time, the OH reorientation time, and the diffusion coefficient at ambient conditions (298.15 K, 1 bar). The calculated activation energies (and their decompositions) are provided in Table 3 and plotted them in Fig. 3.

Measured activation energies have been re-

Table 3: Activation energies (in kcal/mol) of the jump time, OH reorientation time, and diffusion coefficient. Subscripts indicate uncertainties in the trailing digit(s).

Jump Time, τ_0											
Model	Total	KE	Elec	LJ	Bond	Bend	E3B	E_2	E_a	E_b	E_c
SPC/E	3.09_4	0.95_2	2.85_5	-0.72_4	-	-	-	-	-	-	-
SPC/Fw	3.27_6	1.02_2	2.98_{13}	-0.71_5	-0.14_7	0.13_2	-	-	-	-	-
TIP3P-PME	2.71_5	0.88_3	2.30_4	-0.47_3	-	-	-	-	-	-	-
TIP3P-PME/Fw	3.38_6	1.04_3	3.02_{10}	-0.69_5	-0.09_3	0.10_2	-	-	-	-	-
OPC3	3.26_6	0.98_3	3.02_7	-0.74_4	-	-	-	-	-	-	-
E3B2	4.11_6	1.09_3	3.99_5	-1.25_2	-	-	0.28_1	-0.31_1	0.01_1	-0.12_6	0.7_5
E3B3	4.03_2	1.07_4	4.16_{11}	-1.29_5	-	-	0.09_1	-0.04_1	0.01_1	-0.15_2	0.28_2
TIP4P/2005	3.63_5	1.04_4	3.69_8	-1.10_6	-	-	-	-	-	-	
TIP4P/Ew	3.52_6	1.00_3	3.54_8	-1.01_5	-	-	-	-	-	-	
Reorientation Time, τ_2											
Experiment:[69,80] 4.1 ± 0.5, 3.7 ± 0.5 kcal/mol											
Model	Total	KE	Elec	LJ	Bond	Bend	E3B	E_2	E_a	E_b	E_c
SPC/E	3.54_5	1.08_4	3.33_6	-0.86_7	-	-	-	-	-	-	-
SPC/Fw	3.69_9	1.17_5	3.34_{21}	-0.83_9	-0.14_9	0.15_2		- -	-	-	-
TIP3P-PME	2.98_7	0.94_6	2.64_{11}	-0.60_9	-	-	-	-	-	-	-
TIP3P-PME/Fw	3.79_5	1.18_4	3.41_{14}	-0.86_{10}	-0.06_4	0.11_2	-	-	-	-	-
OPC3	3.71_5	1.13_3	3.45_{12}	-0.87_7	-	-	-	-	-	-	-
E3B2	4.69_{10}	1.26_5	4.53_8	-1.42_6	-	-	0.32_2	-0.39_3	-0.04_2	0.39_{13}	0.35_{10}
E3B3	4.55_8	1.24_5	4.66_{11}	-1.44_6	-	-	0.10_1	-0.05_1	0.00_1	-0.06_4	0.21_4
TIP4P/2005	4.12_{10}	1.21_5	4.19_{14}	-1.28_8	-	-	-	-	-	-	-
TIP4P/Ew	3.98_{10}	1.12_5	3.98_{12}	-1.13_8	-	-	-	-	-	-	-
Diffusion Coefficient, D											
Experiment:[49–52,81] 4.2-4.6 kcal/mol											
Model	Total	KE	Elec	LJ	Bond	Bend	E3B	E_2	E_a	E_b	E_c
SPC/E	3.61_9	1.07_4	3.49_{12}	-0.96_6	-	-	-	-	-	-	-
SPC/Fw	3.80_{10}	1.17_3	3.64_{21}	-0.98_7	-0.15_7	0.13_4	-	-	-	-	-
TIP3P-PME	3.26_8	0.94_4	3.14_8	-0.82_3	-	-	-	-	-	-	-
TIP3P-PME/Fw	4.04_8	1.30_5	3.53_{12}	-0.95_6	0.07_4	0.10_3	-	-	-	-	-
OPC3	3.84_7	1.11_3	3.78_{10}	-1.05_6	-	-	-	-	-	-	-
E3B2	4.73_9	1.27_4	4.62_{11}	-1.48_6	-	-	0.31_{11}	-0.52_3	-0.18_2	1.86_{14}	-0.85_{10}
E3B3	4.59_{11}	1.23_5	4.74_{10}	-1.48_8	-	-	0.09_1	-0.07_1	-0.01_1	0.24_3	-0.07_3
TIP4P/2005	4.10_5	1.16_4	4.18_6	-1.24_5	-	-	-	-	-	-	-
TIP4P/Ew	4.03_9	1.14_4	4.10_{12}	-1.21_9	-	-	-	-	-	-	-

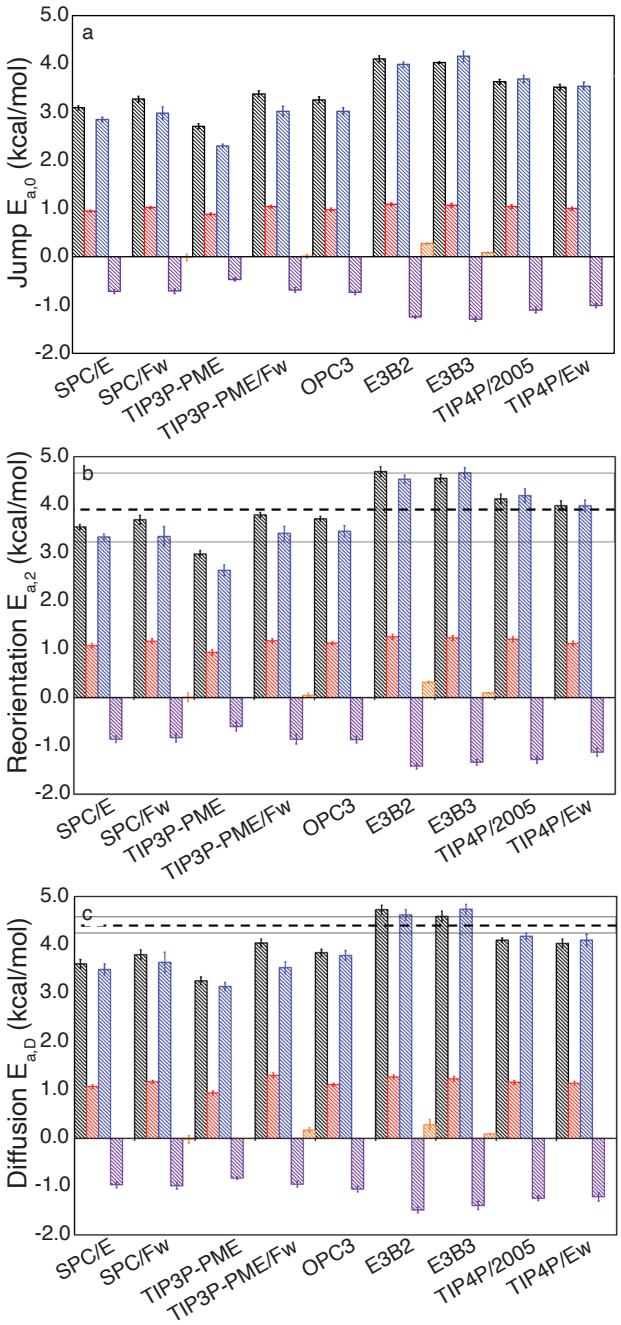

Figure 3: Activation energy decomposition for the studied water models are included for a) the jump time, b) the reorientation time, and c) the diffusion coefficient. The total, kinetic, electrostatic, Lennard-Jones, and other contributions to the activation energy are presented in black, red, blue, purple, and orange, respectively. The experimental values of the diffusion and reorientation activation energies are included as black dashed lines on their respective plots. Experimental uncertainties are included as gray solid lines.

ported for the reorientation time and diffusion coefficient. In the former case, $E_{a,2} = 4.1 \pm 0.5$ kcal/mol was obtained by Petersen *et al.*[69] and 3.7 ± 0.5 kcal/mol by Nicodemus *et al.*[80] Several measurements of the diffusion activation energy have been reported including 4.2,[50] 4.3,[51] 4.4,[49] 4.5,[52] and 4.6 kcal/mol,[81] and thus we take 4.4 kcal/mol as the experimental value in Fig. 3.

We first examine the reorientation activation energies, $E_{a,2}$, which range from 2.98 to 4.69 kcal/mol. All of the models, except TIP3P-PME which has the lowest activation energy, are in agreement, within errors, of one of the reported measured values. However, this is largely due to the significant difference between the two reported experimental $E_{a,2}$ results and their sizable error uncertainties. As with the reorientation timescales, the calculated activation energies appear to fall into two general categories. Namely, the rigid and flexible 3-site models (excepting TIP3P-PME) give $E_{a,2} \simeq 3.5 - 3.8$ kcal/mol, while the 4-site and E3B force fields yield larger activation energies of $4.0 - 4.7$ kcal/mol. Unfortunately, it is not possible to determine which is a better description of the true temperature dependence of liquid water with the currently available experimental data.

The picture for diffusion is somewhat clearer. The TIP3P-PME model gives an $E_{a,D}$ that is lower by more than 0.3 kcal/mol than that for any other force field. Otherwise, the same division of the results into 3-site models that give lower activation energies, $3.6-4.0$ kcal/mol and 4-site and 3-body models that give higher activation energies, $4.0 - 4.7$ kcal/mol is apparent, though with values that overlap. The latter group is in better accord with the measured diffusion activation energy, suggesting that these force fields better represent the temperature dependence of water diffusion.

No experimental value exists to which we can compare the calculated jump activation energies, but we find that the ordering of the activation energies in these models is similar to that of $E_{a,2}$. The TIP3P-PME result lies significantly outside the range of the other models. The 3-site models predict a weaker tem-

perature dependence of the H-bond jump time, $E_{a,0} \simeq 3.1 - 3.4$ kcal/mol compared to the TIP4P- and E3B-based descriptions which give $3.5 - 4.1$ kcal/mol.

We have recently shown[41] that $E_{a,2}$ may be calculated based on the extended jump model,[9,10] which gives it as a contribution from two terms. The first is the contribution due to jumps including $E_{a,0}$ and a measure of the temperature dependence of the size of the angular jump. The second is the activation energy of the unbroken H-bond, or "frame," reorientation obtained from the $C_2(t)$ TCF based on the $O_d \cdots O_a$ vector for H-bonded pairs between jumps. In that work we found that the jump term for the SPC/E model contributed 2.56 kcal/mol to the reorientation activation energy while the frame reorientation added 1.37 kcal/mol. In the present work, we have not calculated these contributions, but it is interesting to consider that different water models might predict different relative jump and frame contributions to $E_{a,2}$.

The addition of 3-body contributions in the E3B2 and E3B3 models raises the activation energies of all three timescales significantly by about $0.4 - 0.7$ kcal/mol compared to the 4-site descriptions. Experimental uncertainty does not allow us to differentiate between these values based on measurements.

The present results indicate that the 4-site and 3-body force fields provide better descriptions of the diffusion coefficient and the corresponding activation energy. The TIP4P/2005 model appears to give the best agreement with measurements of these quantities. This is consistent with its wide use in modeling the T-dependence of water dynamics, including at temperatures far from ambient conditions.[40,82,83] However, as noted above, 3-site models like SPC/E and TIP3P-PME/Fw are superior at describing the OH reorientation time, but unfortunately we cannot use experimental measurements of the associated activation energy to determine if they also properly describe the temperature dependence.

3.3 Activation Energy Decomposition

As we have noted, a key advantage of the fluctuation theory for dynamics approach is the mechanistic insight it generates *via* a rigorous decomposition of the activation energy based on the motions and interactions present in the system. To explore possible differences in the activation energy origins for the different water models we have decomposed them into contributions from the inter- and intramolecular interactions as described in Sec. 2.2.4. The results are given in Table 3 and Fig. 3.

We first note that every model exhibits the same qualitative, even semi-quantitative behavior, in which the dominant contribution is associated with electrostatics, the kinetic energy is a more modest, positive component, and the Lennard-Jones interactions reduce the activation energy. We have previously observed this behavior for the SPC/E and TIP4P/2005 models[35–38,40,41] Specifically, we found that the competition between E_a^{Elec} and E_a^{LJ} can be understood by the interactions involved in breaking an H-bond. During an H-bond exchange, the H-bond acceptor moves out of the first solvation shell of the donor water molecule. This requires an increase in the electrostatic energy between the two molecules but a decrease in the Lennard-Jones interactions, which lie on the repulsive wall of the potential in the intact H-bond. The present results indicate that, despite the relatively wide ranges of timescales and activation energies calculated from these models, they treat the underlying competition between these contributions in a similar way.

Considering specifically the kinetic energy contribution to the activation energies, we see (Table 3) that it lies in the range $0.88 - 1.3$ kcal/mol over the full set of models and timescales. The smallest kinetic energy contributions occur for the TIP3P-PME model in every case, which we noted above significantly underestimates every activation energy. Ignoring this model we find that the range of values is even smaller for a given timescale where for the jump time $E_{a,0}^{KE} = 0.95 - 1.09$ kcal/mol, for the reorientation time $E_{a,2}^{KE} = 1.08 -$

1.26 kcal/mol, and for the diffusion coefficient $E_{a,D}^{KE} = 1.07 - 1.30$ kcal/mol. While these differences are small, the E3B models consistently have the largest kinetic energy contribution and the SPC/E, OPC3, and TIP4P/Ew force fields have the smallest.

Examination of the electrostatic contributions also yields a consistent picture. It is not only the largest contribution but quite close to the total activation energy, within $\sim$ 0.4 kcal/mol, in every case. In this way it closely tracks the trends in the activation energy for the different models that are discussed above. As would be expected from the physical picture of competition between the electrostatic and Lennard-Jones interactions we have just described, we find E_a^{Elec} and E_a^{LJ} are anti-correlated. Smaller electrostatic contributions, which occur particularly for the rigid and flexible 3-site models, are accompanied by smaller in magnitude (less negative) Lennard-Jones components. In contrast, for the 4-site and 3-body force fields we find the electrostatic component of the activation energy is larger and the corresponding Lennard-Jones term is bigger in magnitude (more negative).

It is also interesting to consider the other contributions to the activation energy associated with flexibility or 3-body interactions that are not shared by every model. Interestingly, the bending and stretching contributions to the activation energy of SPC/Fw essentially cancel each other for every timescale so that the molecular flexibility has no direct effect on the activation energy. This is also true for the TIP3P-PME/Fw model for the jump and reorientation time activation energies, but they combine to increase $E_{a,D}$ in the case of diffusion. More importantly, these results indicate that the differences in the E_a predicted by the SPC/E and SPC/Fw models, which are modest, and those between the TIP3P-PME and TIP3P-PME/Fw models, which are significant, must be attributed to underlying changes in the liquid structure induced by the addition of flexibility rather than a direct role in the dynamics.

In the E3B2 and E3B3 models, the activation energy contributions that come from the addition of 3-body interactions likewise do not

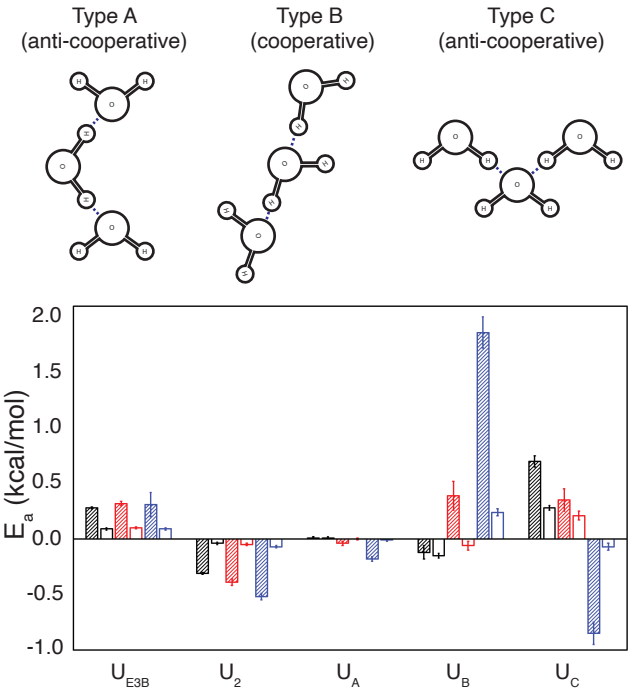

Figure 4: Contributions to the jump (black), reorientation (red), and diffusion (blue) activation energies for the E3B model components (U_2, U_A, U_B and U_C) for the E3B2 (striped bars) and the E3B3 (empty bars) models.

add up to the total difference in the activation energy when compared with their base models (TIP4P/2005 for E3B3). Indeed, the 3-body terms add $\sim$ 0.3 and 0.1 kcal/mol to the activation energy of each timescale for the E3B2 and E3B3 model, respectively. Note that, in the case where a direct comparison is possible, the overall activation energies are $0.39 - 0.43$ kcal/mol higher for the E3B3 force field than for the base TIP4P/2005 description. Thus, as was the case for the effect of molecular flexibility, it is apparent that the key effect of including 3-body interactions is the modification of the liquid structure.

The 3-body contribution to the activation energy can be further decomposed into the components due to the many-body correction to the pairwise potential ($E_a^{U_2}$), anti-cooperative arrangements ($E_a^{U_A}$ and $E_a^{U_C}$), and cooperative arrangements ($E_a^{U_B}$). We have plotted this decomposition for both E3B2 and E3B3 in Fig. 4 along with a schematic illustration of the latter three interactions. For both models, the

$E_a^{U_2}$ represents a small negative contribution to the activation energy, but the magnitude for E3B2 is significantly greater than that of E3B3. Because the U_2 term is designed to remove the many-body effects implicitly included in the base pairwise force field,[28,29] this term provides insight into the approximate magnitude of the base model activation energy associated with those many-body effects. Thus, the negative values of $E_a^{U_2}$ indicates that the base 4-site potentials (TIP4P, TIP4P/2005) would have lower activation energies if many-body effects were not included implicitly.

For both models, the anti-cooperative arrangement term $E_a^{U_A}$ contributes the least to the activation energy, with only reorientation and diffusion having slight negative contributions for the E3B2 model. This suggests that the base 4-site models accurately describe the T-dependence of the Type A, anti-cooperative, arrangements without explicit inclusion of 3-body effects. The majority of the remaining contribution to the activation energy comes from the Type B and Type C arrangements, which are (generally) in opposition to one another for each timescale. Interestingly, the Type B (cooperative) configurations appear to strongly increase the T-dependence of the diffusion coefficient, while decreasing the T-dependence of the jump time. Meanwhile, the Type C (anti-cooperative) configurations display the opposite effect. The reorientation activation energy displays behavior intermediate between that of the H-bond jump time and the diffusion coefficient.

3.4 Activation Volumes

Finally, we examine the pressure dependence of the dynamical timescales predicted by the different water models as represented by the activation volumes. Specifically, we have calculated the activation volumes at 298.15 K and 1 bar of the H-bond jump time, OH reorientation time, and diffusion coefficient. The values are provided in Table 4 and the results are plotted in Fig. 5. We compare with experimental results based on fitting to NMR measurements of D at a series of pressures.[49,53,84] Recently, Fanetti

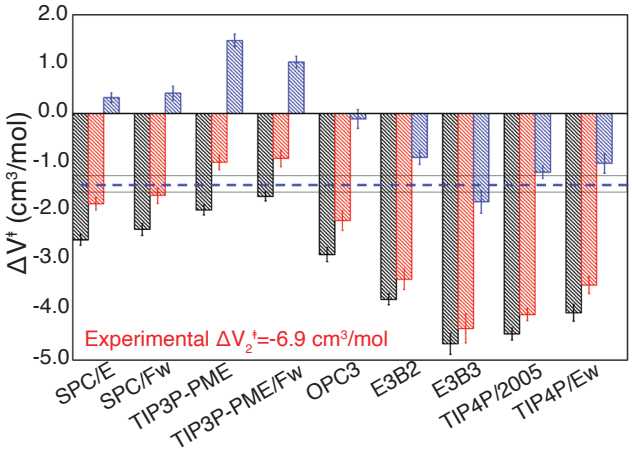

Figure 5: Activation volumes of the jump time, $\Delta V_0^\ddagger$ (black), reorientation time, $\Delta V_2^\ddagger$ (red), and diffusion coefficient, $\Delta V_D^\ddagger$ (blue). The average experimental diffusion activation volume[49,53,84] is also shown (dashed blue line; experimental ranges indicated by gray solid lines). The experimental reorientation activation volume at 450 bar is also listed.[85]

et al. have published pump-probe anisotropy measurements of the reorientation time over a wide range of pressures.[85] We have used their values of the reorientation time at 1 bar, 600 bar, and 900 bar to evaluate the reorientation activation volume ($\Delta V_2^\ddagger$) numerically, for which we have found a value of -6.9 cm^3/mol. To the best of our knowledge, this is the first experimental value for the activation volume of the τ_2 timescale. We are unaware of any measurements for τ_0.

We first note the general features of the results. We find that the activation volumes for the H-bond jump time, $\Delta V_0^\ddagger$, and the OH reorientation time, $\Delta V_2^\ddagger$ are negative for all of the models and that, in every case, $\Delta V_0^\ddagger$ is larger in magnitude (more negative) than $\Delta V_2^\ddagger$. The negative activation volumes here correspond to an increase (decrease) in the corresponding rate constant (timescale) with increasing pressure. However, for the diffusion coefficient the 3-site models predict an activation volume that is positive or zero (within errors) but the 4-site and 3-body models yield a negative activation volume. This is an interesting contrast with the activation energy, where we observed comparatively small quantitative differences between

Table 4: Activation volumes (in cm^3/mol) of the jump time, $\Delta V_0^\ddagger$, reorientation time, $\Delta V_2^\ddagger$ and diffusion coefficient, $\Delta V_D^\ddagger$. Subscripts indicate uncertainties in the trailing digit(s).

Model	$\Delta V_0^\ddagger$	$\Delta V_2^\ddagger$	$\Delta V_D^\ddagger$
SPC/E	-2.56_{11}	-1.83_{13}	0.32_{10}
SPC/Fw	-2.35_{12}	-1.66_{16}	0.41_{14}
TIP3P-PME	-1.96_{10}	-0.99_{15}	1.48_{13}
TIP3P-PME/Fw	-1.68_{9}	-0.91_{17}	1.04_{12}
OPC3	-2.86_{14}	-2.17_{20}	-0.11_{19}
E3B2	-3.77_{11}	-3.36_{21}	-0.89_{14}
E3B3	-4.67_{21}	-4.36_{29}	-1.79_{23}
TIP4P/2005	-4.47_{12}	-4.08_{12}	-1.19_{13}
TIP4P/Ew	-4.04_{17}	-3.48_{17}	-1.01_{20}
Expt.[49,53,84,85]	-	-6.9[a]	(-1.3)-(-1.6)

[a] At 450 bar.

the results for the different timescales, particularly for $E_{a,2}$ and $E_{a,D}$. We note that the diffusion activation volume, $\Delta V_D^\ddagger$, changes sign with both pressure and temperature,[51,72] so that the quantitative results here apply only for the ambient conditions at which they were evaluated.

While the experimental $\Delta V_2^\ddagger$ for reorientation is not centered around 1 bar,[85] it is still in reasonable agreement with our calculated results. Importantly, it suggests that the stronger pressure effect observed in the simulations for the reorientation time compared to the diffusion coefficient matches the available experimental data showing $|\Delta V_2^\ddagger| > |\Delta V_D^\ddagger|$. Fanetti *et al.* also reported the p-dependence of τ_2 for the ASAP water force-field,[86] using their values and an Arrhenius-type numerical procedure we estimate an activation volume of $\Delta V_2^\ddagger = -3.7$ cm^3/mol, which is in general agreement with the present, directly calculated, results for different models.

We note that the activation volume measures the difference in volume of the transition state and reactant structures, broadly defined in that it contains any changes in the surrounding solvent arrangement as well.[87] Thus, a negative (positive) activation volume corresponds to a reduction (increase) in size moving from the reactant state to the transition state. The present results suggest that the volume of the transition state for diffusion is distinctly different than that for reorientation and H-bond jumps despite the fact that the activation energies are quite similar. The latter is understood as a signature of the fact that both reorientation and diffusion have H-bond exchanges as their underlying fundamental process. A key difference between the processes is that diffusion has a component associated with a translational jump accompanying the exchange[59] while reorientation involves one due to an angular jump. While an extended jump model has been developed for OH reorientation,[9,10] a similar rigorous description is lacking for diffusion; the present results indicate that an accurate reproduction of the diffusion activation volume and its connection to the jump activation volume should be key targets of such a model.

Comparing the results from the different water models does give a consistent picture across the three timescales. Namely, the 3-site models predict larger (positive or less negative) activation volumes in all cases. For diffusion, this means that the 3-site models incorrectly predict the relative size of the transition state and reactant arrangements. The 4-site and 3-body models give $\Delta V_D^\ddagger \simeq -0.9$ to -1.8 cm^3/mol, which is in reasonable agreement with the range of experimental values. The TIP4P/2005 (-1.19 ± 0.13 cm^3/mol) and E3B3 (-1.79 ± 0.23 cm^3/mol) force fields give the overall best results and the only ones that overlap, within error, with the measurements.

In the case of the activation volumes for τ_0 and τ_2, the 3-site models are quantitatively, but not qualitatively, different. They predict negative activation volumes, but ones that are as much as $3-4$ times smaller than the 4-site and 3-body models. Interestingly, the two 3-body models yield significantly different activation volumes, with the E3B2 model giving results $\sim 0.9 - 1.0$ cm^3/mol larger than the E3B3 values for every timescale. This leads to E3B2 activation volumes that are less negative than the 4-site (TIP4P/2005 and TIP4P/Ew) models, but more negative E3B3 activation volumes. It is tempting to speculate that this is associated with the larger contributions of the Type B and Type C configurations in the E3B2 model as observed in the activation energy de-

compositions, Fig. 4, but we do not currently have an approach for evaluating such a hypothesis.

The TIP3P-PME and TIP3P-PME/Fw models are the largest outliers as they predict the most positive $\Delta V_D^\ddagger$ and the smallest magnitude $\Delta V_0^\ddagger$ and $\Delta V_2^\ddagger$. The diffusion result is furthest from the measured values and indicates that these force fields do not adequately describe the pressure dependence. It is interesting that, while the TIP3P-PME/Fw model substantially improves on the deficiencies of TIP3P-PME with respect to timescales (Table 2) and activation energies (Table 3), it does not notably improve upon the pressure dependence.

4 Conclusions

In the present work, we have used dynamical fluctuation theory to evaluate the timescales, activation energies, and activation volumes of the H-bond exchange, or "jump," time, the OH reorientation time, and the diffusion coefficient for several commonly used water models. While these timescales are non-Arrhenius in water, these activation parameters provide a good measure of the local temperature/pressure dependencies (for example, the activation energy provides a good estimate for the T-dependence[40] of these timescales over a range $\sim 280 - 340$ K). To our knowledge, this is the first calculation of the jump and reorientation activation volumes. We do note that, in this first comparison between models, we have not considered polarizable models, models with more than four sites, electronic structure-based descriptions, or potentials that include more than 3-body effects,[88] which could provide improvement to some or all of the quantities calculated in the present work.

The results show that SPC/E, SPC/Fw, and TIP3P-PME/Fw provide the best description of reorientation timescales in liquid water whereas TIP4P/2005 most faithfully reproduces the measured diffusion coefficient. The four-site and three-body models more accurately predict the diffusion activation energy, and thus at least the local temperature dependence of diffusion, compared to any of the 3-site models. The TIP3P-PME force field does a universally poor job of describing timescales, activation energies, and activation volumes. We are unable to distinguish between the other models based on the reorientation or jump time activation energies, due to the significant uncertainty in the experimental result for the former and the lack of measurements for the latter.

We have decomposed the activation energies and found that all of the models share the same underlying mechanistic origin of the water dynamics. Namely, a strong competition is observed between the electrostatic and Lennard-Jones interactions with the former representing the dominant contribution. Molecular flexibility and 3-body effects both provide a small direct contribution to the activation energy, but also lead to other changes, e.g., in the liquid structure, that more significantly affect the activation energy.

The superior description of the four-site and 3-body models also extends to the pressure dependence, where the activation volumes for both the reorientation time and diffusion coefficient are in significantly better agreement with experiment than those of the 3-site models. Surprisingly, the activation volumes for the OH reorientation and H-bond jump times are substantially more negative than those for the diffusion coefficient.

Overall, of the force fields examined, TIP4P/2005 and E3B3 (which adds three-body interactions to the TIP4P/2005 model) give the best representation of the dynamical properties and their temperature and pressure dependence. However, this conclusion comes with qualifications. These models overestimate the OH reorientation timescale (and presumably the H-bond jump time) while simultaneously matching experimental measurements of the diffusion coefficient, its activation energy, and its activation volume. The reorientation time is more accurately predicted by the three-site SPC/E, SPC/Fw, and TIP3P-PME/Fw models that, however, predict diffusion that is too fast and a diffusion activation energy that is too low.

Acknowledgements

The authors would like to thank Prof. Brian B. Laird, Prof. Damien Laage, and Dr. Steven Strong for useful discussions. The authors are grateful to Drs. Andrea Lapini and Roberto Bini for sharing their reorientation dynamics data. This work was supported by the National Science Foundation under Grant No. CHE-1800559. This material is based on the work supported by the National Science Foundation Graduate Research Fellowship under Grant Nos. 1540502 and 1451148 as well as the National Science Graduate Research Opportunities Worldwide Program. The calculations were performed at the University of Kansas Center for Research Computing (CRC).

Data Availability

The data that support the findings of this study are available from the corresponding author upon reasonable request.

Supporting Information

We have made the program used for dynamical fluctuation theory (which work with the SLURM queue engine and LAMMPS) available at the following DOI: 10.5281/zenodo.4064073.[89] Note that some basic modifications of this code may be required depending on particular cluster/environments. LAMMPS input files for the NpT and NVE trajectories are included in SI-Input-Files.txt.

References

(1) Berendsen, H. J.; Grigera, J. R.; Straatsma, T. P. The missing term in effective pair potentials. *J. Phys. Chem* **1987**, *91*, 6269–6271.

(2) Wu, Y.; Tepper, H. L.; Voth, G. A. Flexible simple point-charge water model with improved liquid-state properties. *J. Chem. Phys.* **2006**, *124*, 024503.

(3) Abascal, J. L.; Vega, C. A general purpose model for the condensed phases of water: TIP4P/2005. *J. Chem. Phys.* **2005**, *123*, 234505.

(4) Horn, H. W.; Swope, W. C.; Pitera, J. W.; Madura, J. D.; Dick, T. J.; Hura, G. L.; Head-Gordon, T. Development of an improved four-site water model for biomolecular simulations: TIP4P-Ew. *J. Chem. Phys.* **2004**, *120*, 9665–9678.

(5) Joung, I. S.; Cheatham, T. E. Determination of alkali and halide monovalent ion parameters for use in explicitly solvated biomolecular simulations. *J. Phys. Chem. B.* **2008**, *112*, 9020–9041.

(6) Jorgensen, W. L.; Chandrasekhar, J.; Madura, J. D.; Impey, R. W.; Klein, M. L. Comparison of simple potential functions for simulating liquid water. *J. Chem. Phys.* **1983**, *79*, 926–935.

(7) Nutt, D. R.; Smith, J. C. Molecular dynamics simulations of proteins: Can the explicit water model be varied? *J. Chem. Theory Comput.* **2007**, *3*, 1550–1560.

(8) Best, R. B.; Mittal, J. Protein simulations with an optimized water model: Cooperative helix formation and temperature-induced unfolded state collapse. *J. Phys. Chem. B.* **2010**, *114*, 14916–14923.

(9) Laage, D.; Hynes, J. T. A molecular jump mechanism of water reorientation. *Science* **2006**, *311*, 832–835.

(10) Laage, D.; Hynes, J. T. On the molecular mechanism of water reorientation. *J. Phys. Chem. B* **2008**, *112*, 14230–14242.

(11) Laage, D.; Hynes, J. T. In *Ultrafast Infrared Vibrational Spectroscopy*; Fayer, M. D., Ed.; CRC Press, 2013; pp 73–98.

(12) Paesani, F. Temperature-dependent infrared spectroscopy of water from a first-principles approach. *J. Phys. Chem. A.* **2011**, *115*, 6861–6871.

(13) Cisneros, G. A.; Wikfeldt, K. T.; Ojamäe, L.; Lu, J.; Xu, Y.; Torabifard, H.; Bartók, A. P.; Csányi, G.; Molinero, V.; Paesani, F. Modeling molecular interactions in water: From pairwise to many-body potential energy functions. *Chem. Rev.* **2016**, *116*, 7501–7528.

(14) Asbury, J. B.; Steinel, T.; Stromberg, C.; Corcelli, S. A.; Lawrence, C. P.; Skinner, J. L.; Fayer, M. D. Water dynamics: Vibrational echo correlation spectroscopy and comparison to molecular dynamics simulations. *J. Phys. Chem. A* **2004**, *108*, 1107–1119.

(15) Møller, K. B.; Rey, R.; Hynes, J. T. Hydrogen bond dynamics in water and ultrafast infrared spectroscopy: A theoretical study. *Journal of Physical Chemistry A* **2004**, *108*, 1275–1289.

(16) Brini, E.; Fennell, C. J.; Fernandez-Serra, M.; Hribar-Lee, B.; Lukšič, M.; Dill, K. A. How water's properties are encoded in its molecular structure and energies. *Chem. Rev.* **2017**, *117*, 12385–12414.

(17) Singh, R. S.; Biddle, J. W.; Debenedetti, P. G.; Anisimov, M. A. Two-state thermodynamics and the possibility of a liquid-liquid phase transition in supercooled TIP4P/2005 water. *J. Chem. Phys.* **2016**, *144*, 144504.

(18) Hestand, N. J.; Skinner, J. L. Perspective: Crossing the Widom line in no man's land: Experiments, simulations, and the location of the liquid-liquid critical point in supercooled water. *J. Chem. Phys.* **2018**, *149*, 140901.

(19) Gallo, P.; Amann-Winkel, K.; Angell, C. A.; Anisimov, M. A.; Caupin, F.; Chakravarty, C.; Lascaris, E.; Loerting, T.; Panagiotopoulos, A. Z.; Russo, J.; Sellberg, J. A.; Stanley, H. E.; Tanaka, H.; Vega, C.; Xu, L.; Pettersson, L. G. M. Water: A tale of two liquids. *Chem. Rev.* **2016**, *116*, 7463–7500.

(20) Palmer, J. C.; Poole, P. H.; Sciortino, F.; Debenedetti, P. G. Advances in computational studies of the liquid-liquid transition in water and water-like models. *Chem. Rev.* **2018**, *118*, 9129–9151.

(21) Lata, N. N.; Zhou, J.; Hamilton, P.; Larsen, M.; Sarupria, S.; Cantrell, W. Multivalent surface cations enhance heterogeneous freezing of water on muscovite mica. *J. Phys. Chem. Lett.* **2020**, *11*, 8682–8689.

(22) Bellissent-Funel, M. C.; Hassanali, A.; Havenith, M.; Henchman, R.; Pohl, P.; Sterpone, F.; Van Der Spoel, D.; Xu, Y.; Garcia, A. E. Water determines the structure and dynamics of proteins. *Chem. Rev.* **2016**, *116*, 7673–7697.

(23) Kohagen, M.; Pluhaová, E.; Mason, P. E.; Jungwirth, P. Exploring ion-ion interactions in aqueous solutions by a combination of molecular dynamics and neutron scattering. *J. Phys. Chem. Lett.* **2015**, *6*, 1563–1567.

(24) Laage, D.; Elsaesser, T.; Hynes, J. T. Water dynamics in the hydration shells of biomolecules. *Chem. Rev.* **2017**, *117*, 10694–10725.

(25) Harpham, M. R.; Ladanyi, B. M.; Levinger, N. E. The effect of the counterion on water mobility in reverse micelles studied by molecular dynamics simulations. *J. Phys. Chem. B.* **2005**, *109*, 16891–16900.

(26) Yamada, S. A.; Shin, J. Y.; Thompson, W. H.; Fayer, M. D. Water dynamics in nanoporous silica: Ultrafast vibrational spectroscopy and molecular dynamics simulations. *J. Phys. Chem. C.* **2019**, *123*, 5790–5803.

(27) Izadi, S.; Onufriev, A. V. Accuracy limit of rigid 3-point water models. *J. Chem. Phys.* **2016**, *145*, 074501.

(28) Tainter, C. J.; Pieniazek, P. A.; Lin, Y. S.; Skinner, J. L. Robust three-body water

simulation model. *J. Chem. Phys.* **2011**, *134*, 184501.

(29) Tainter, C. J.; Shi, L.; Skinner, J. L. Reparametrized E3B (explicit three-body) water model using the TIP4P/2005 model as a reference. *J. Chem. Theory Comput.* **2015**, *11*, 2268–2277.

(30) Drljaca, A.; Hubbard, C. D.; van Eldik, R.; Asano, T.; Basilevsky, M. V.; le Noble, W. J. Activation and reaction volumes in solution. 3. *Chem. Rev.* **1998**, *98*, 2167–2290.

(31) Annapureddy, H. V. R.; Dang, L. X. Water exchange rates and molecular mechanism around aqueous halide ions. *J. Phys. Chem. B* **2014**, *118*, 7886–7891.

(32) Dang, L. X.; Schenter, G. K. Solvent exchange in liquid methanol and rate theory. *Chem. Phys. Lett.* **2016**, *643*, 142–148.

(33) Price, D. J.; Brooks, C. L. A modified TIP3P water potential for simulation with Ewald summation. *J. Chem. Phys.* **2004**, *121*, 10096–10103.

(34) Mesele, O. O.; Thompson, W. H. Removing the barrier to the calculation of activation energies. *J. Chem. Phys.* **2016**, *145*, 13410.

(35) Piskulich, Z. A.; Mesele, O. O.; Thompson, W. H. Removing the barrier to the calculation of activation energies: Diffusion coefficients and reorientation times in liquid water. *J. Chem. Phys.* **2017**, *147*, 134103.

(36) Piskulich, Z. A.; Thompson, W. H. The activation energy for water reorientation differs between IR pump-probe and NMR measurements. *J. Chem. Phys.* **2018**, *149*, 164504.

(37) Piskulich, Z. A.; Mesele, O. O.; Thompson, W. H. Activation energies and beyond. *J. Phys. Chem. A.* **2019**, *123*, 7185–7194.

(38) Mendis, C.; Piskulich, Z. A.; Thompson, W. H. Tests of the Stokes-Einstein relation through the shear viscosity activation energy of water. *J. Phys. Chem. B.* **2019**, *123*, 5857–5865.

(39) Piskulich, Z. A.; Thompson, W. H. On the temperature dependence of liquid structure. *J. Chem. Phys.* **2020**, *152*, 011102.

(40) Piskulich, Z. A.; Thompson, W. H. The dynamics of supercooled water can be predicted from room temperature simulations. *J. Chem. Phys.* **2020**, *152*, 074505.

(41) Piskulich, Z. A.; Laage, D.; Thompson, W. H. Activation energies and the extended jump model : How temperature affects reorientation and hydrogen-bond exchange dynamics in water. *J. Chem. Phys.* **2020**, *153*, 074110.

(42) Piskulich, Z. A.; Thompson, W. H. Temperature dependence of the water infrared spectrum: Driving forces, isosbestic points, and predictions. *J. Phys. Chem. Lett.* **2020**, *11*, 7762–7768.

(43) Sun, H. Compass: An ab initio forcefield optimized for condensed-phase applications - Overview with details on alkane and benzene compounds. *Journal of Physical Chemistry B* **1998**, *102*, 7338–7364.

(44) Darden, T.; York, D.; Pedersen, L. Particle mesh Ewald: An N·log(N) method for Ewald sums in large systems. *J. Chem. Phys.* **1993**, *98*, 10089–10092.

(45) Pollock, E. L.; Glosli, J. Comments on PPPM, FMM, and the Ewald Method for Large Periodic Coulombic Systems. *Comput. Phys. Comm.* **1995**, *95*, 93–110.

(46) Ryckaert, J. P.; Ciccotti, G.; Berendsen, H. J. Numerical integration of the cartesian equations of motion of a system with constraints: molecular dynamics of n-alkanes. *J. Comput. Phys.* **1977**, *23*, 327–341.

(47) Piskulich, Z. A.; Mesele, O. O.; Thompson, W. H. Expanding the calculation of activation volumes: Self-diffusion in liquid water. *J. Chem. Phys.* **2018**, *148*, 134105.

(48) Qvist, J.; Schober, H.; Halle, B. Structural dynamics of supercooled water from quasielastic neutron scattering and molecular simulations. *J. Chem. Phys.* **2011**, *134*, 144508.

(49) Woolf, L. A. Tracer diffusion of tritiated water (THO) in ordinary water (H_2O) under pressure. *J. Chem. Soc., Faraday Trans. 1* **1975**, *71*, 784–796.

(50) Mills, R. Self-diffusion in normal and heavy water in the range $1-45°$. *J. Phys. Chem.* **1973**, *77*, 685–688.

(51) Krynicki, K.; Green, C. D.; Sawyer, D. W. Pressure and temperature dependence of self-diffusion in water. *Faraday Discuss. Chem. Soc.* **1978**, *66*, 199–208.

(52) Gillen, K. T.; Douglass, D. C.; Hoch, M. J. Self-diffusion in liquid water to $-31°$C. *J. Chem. Phys.* **1972**, *57*, 5117–5119.

(53) Harris, K. R.; Newitt, P. J. Self-diffusion of water at low temperatures and high pressure. *J. Chem. Eng. Data* **1997**, *42*, 346–348.

(54) Chen, S.-H.; Mallamace, F.; Mou, C.-Y.; Broccio, M.; Corsaro, C.; Faraone, A.; Liu, L. The violation of the Stokes-Einstein relation in supercooled water. *Proc. Natl. Acad. Sci.* **2006**, *103*, 12974–12978.

(55) Dunweg, B.; Kremer, K. Molecular dynamics simulation of a polymer chain in solution. *J. Chem. Phys.* **1993**, *99*, 6983–6997.

(56) Yeh, I.-C.; Hummer, G. System-size dependence of diffusion coefficients and viscosities from molecular dynamics simulations with periodic boundary conditions. *J. Phys. Chem. B* **2004**, *108*, 15873–15879.

(57) Lin, Y. S.; Pieniazek, P. A.; Yang, M.; Skinner, J. L. On the calculation of rotational anisotropy decay, as measured by ultrafast polarization-resolved vibrational pump-probe experiments. *J. Chem. Phys.* **2010**, *132*, 174505.

(58) Gordon, R. G. Relations between Raman spectroscopy and nuclear spin relaxation. *J. Chem. Phys.* **1965**, *42*, 3658–3665.

(59) Glasstone, S.; K.J., L.; Eyring, H. In *The Theory of Rate Processes*; McGraw-Hill,, Ed.; 1941.

(60) Linke, M.; Köfinger, J.; Hummer, G. Rotational Diffusion Depends on Box Size in Molecular Dynamics Simulations. *Journal of Physical Chemistry Letters* **2018**, *9*, 2874–2878.

(61) Tolman, R. C. Statistical mechanics applied to chemical kinetics. *J. Am. Chem. Soc* **1920**, *42*, 2506–2528.

(62) Martinez, L.; Andrade, R.; Birgin, E.; Martinez, J. Packmol: A package for building initial configurations. *J. Comput. Chem.* **2009**, *30*, 2157–2164.

(63) Plimpton, S. Fast parallel algorithms for short-range molecular dynamics. *J. Comput. Phys.* **1995**, *117*, 1–19.

(64) Shinoda, W.; Shiga, M.; Mikami, M. Rapid estimation of elastic constants by molecular dynamics simulation under constant stress. *Phys. Rev. B.* **2004**, *69*, 16–18.

(65) Martyna, G. J.; Tobias, D. J.; Klein, M. L. Constant pressure molecular dynamics algorithms. *J. Chem. Phys.* **1994**, *101*, 4177–4189.

(66) Nosé, S. A unified formulation of the constant temperature molecular dynamics methods. *J. Chem. Phys.* **1984**, *81*, 511–519.

(67) Hoover, W. G. Canonical dynamics: Equilibrium phase-space distributions. *Phys. Rev. A* **1985**, *31*, 1695–1697.

(68) Shoemaker, D. P.; Garland, C. W.; Nibler, J. W. *Experiments in physical chemistry*; McGraw-Hill: New York, 1989.

(69) Petersen, C.; Tielrooij, K. J.; Bakker, H. J. Strong temperature dependence of water reorientation in hydrophobic hydration shells. *J. Chem. Phys.* **2009**, *130*, 214511.

(70) Moilanen, D. E.; Fenn, E. E.; Lin, Y.-S.; Skinner, J. L.; Bagchi, B.; Fayer, M. D. Water inertial reorientation: Hydrogen bond strength and the angular potential. *Proc. Natl. Acad. Sci. USA* **2008**, *105*, 5295–5300.

(71) Ramasesha, K.; Roberts, S. T.; Nicodemus, R. A.; Mandal, A.; Tokmakoff, A. Ultrafast 2D IR anisotropy of water reveals reorientation during hydrogen-bond switching. *J. Chem. Phys.* **2011**, *135*, 054509.

(72) Weingartner, H. Self-Diffusion in liquid water. A reassessment. *Z. Phys. Chem.* **1982**, *132*, 129–149.

(73) Cho, C. H.; Urquidi, J.; Singh, S.; Robinson, G. W. Thermal offset viscosities of liquid H_2O, D_2O, and T_2O. *J. Phys. Chem. B* **1999**, *103*, 1991–1994.

(74) Vega, C.; Abascal, J. L.; Conde, M. M.; Aragones, J. L. What ice can teach us about water interactions: A critical comparison of the performance of different water models. *Faraday Disc.* **2008**, *141*, 251–276.

(75) González, M. A.; Abascal, J. L. The shear viscosity of rigid water models. *J. Chem. Phys.* **2010**, *132*, 096101.

(76) Guevara-Carrion, G.; Vrabec, J.; Hasse, H. Prediction of self-diffusion coefficient and shear viscosity of water and its binary mixtures with methanol and ethanol by molecular simulation. *J. Chem. Phys.* **2011**, *134*, 074508.

(77) Vega, C.; Abascal, J. L. Simulating water with rigid non-polarizable models: A general perspective. *Phys. Chem. Chem. Phys.* **2011**, *13*, 19663–19688.

(78) Mark, P.; Nilsson, L. Structure and dynamics of the TIP3P, SPC, and SPC/E water models at 298 K. *J. Phys. Chem. A* **2001**, *105*, 9954–9960.

(79) van der Spoel, D.; van Maaren, P. J.; Berendsen, H. J. C. A systematic study of water models for molecular simulation: Derivation of water models optimized for use with a reaction field. *J. Chem. Phys.* **1998**, *108*, 10220–10230.

(80) Nicodemus, R. A.; Corcelli, S. A.; Skinner, J. L.; Tokmakoff, A. Collective hydrogen bond reorganization in water studied with temperature-dependent ultrafast infrared spectroscopy. *J. Phys. Chem. B.* **2011**, *115*, 5604–5616.

(81) Pruppacher, H. R. Self-diffusion coefficient of supercooled water. *J. Chem. Phys.* **1972**, *56*, 101–107.

(82) Kawasaki, T.; Kim, K. Identifying time scales for violation/preservation of Stokes-Einstein relation in supercooled water. *Sci. Adv.* **2017**, *2017*, 1–8.

(83) Saito, S.; Bagchi, B.; Ohmine, I. Crucial role of fragmented and isolated defects in persistent relaxation of deeply supercooled water. *J. Chem. Phys.* **2018**, *149*, 124504.

(84) Harris, K. R.; Woolf, L. A. Pressure and temperature dependence of the self diffusion coefficient of water and oxygen-18 water. *J. Chem. Soc., Faraday Trans. 1* **1980**, *76*, 377–385.

(85) Fanetti, S.; Lapini, A.; Pagliai, M.; Citroni, M.; Di Donato, M.; Scandolo, S.; Righini, R.; Bini, R. Structure and dynamics of low-density and high-density liquid water at high pressure. *J. Phys. Chem. Lett.* **2014**, *5*, 235–240.

(86) Pinilla, C.; Irani, A. H.; Seriani, N.; Scandolo, S. Ab initio parameterization of an

all-atom polarizable and dissociable force field for water. *J. Chem. Phys.* **2012**, *136*, 114511.

(87) Ladanyi, B. M.; Hynes, J. T. Transition-state solvent effects on atom transfer rates in solution. *J. Am. Chem. Soc* **1986**, *108*, 585–593.

(88) Reddy, S. K.; Straight, S. C.; Bajaj, P.; Huy Pham, C.; Riera, M.; Moberg, D. R.; Morales, M. A.; Knight, C.; Götz, A. W.; Paesani, F. On the accuracy of the MB-pol many-body potential for water: Interaction energies, vibrational frequencies, and classical thermodynamic and dynamical properties from clusters to liquid water and ice. *J. Chem. Phys.* **2016**, *145*, 194504.

(89) Piskulich, Z. A.; Thompson, W. H. Fluctuation Theory for Dynamics. DOI: 10.5281/zenodo.4064073, 2020.

TOC Graphic

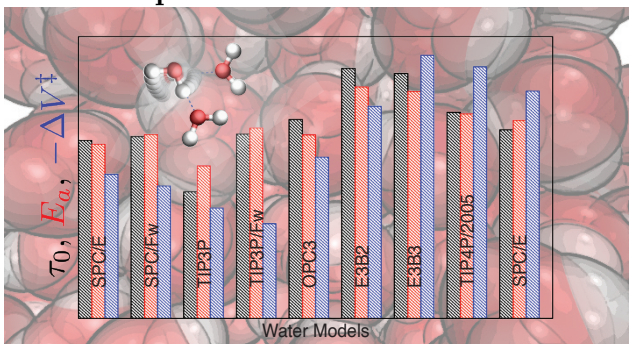
τ_0, E_a, $-\Delta V^{\ddagger}$
SPC/E
SPC/Fw
TIP3P
TIP3P/Fw
OPC3
E3B2
E3B3
TIP4P/2005
SPC/E
Water Models